

A Dual Band Eight Port MIMO Antenna with EBG metamaterial for V2X Application

Maruti R. Jadhav* and Uttam L. Bombale

Shivaji University, Kolhapur, India

ABSTRACT: Several communication systems use multiple input and multiple output (MIMO) antennas to rapidly broadcast and receive data streams. Several current research works on MIMO antennas for vehicle-to-everything (V2X) applications were detailed, along with some limitations such as significant mutual coupling and antenna isolation. To address these difficulties, the manuscript presented a novel metamaterial-based dual-band eight-port MIMO antenna for V2X applications. The proposed eight-port MIMO antenna could be applied to V2X applications in the frequency range of 5.6 GHz to 5.8 GHz. The antenna could resonate at two frequencies, namely 5.64 GHz and 5.73 GHz. The MIMO antenna was constructed with a polyimide substrate and a coplanar waveguide feed (CWF) line. To attain better isolation, a plus shape defected ground structure (Plus shape DGS) was used in this research. By using the binary waterwheel plant optimization algorithm, the antenna parameters are optimized. The proposed antenna was analyzed under different parameters such as gain, return loss, Voltage Standing Wave Ratio (VSWR), axial ratio, and other diversity performances of MIMO antenna like envelope correlation coefficient (ECC), Total Active Reflection Coefficient (TARC), Mean Effective Coefficient (MEG), and Diversity Gain (DG). The proposed antenna is used in a binary waterwheel plant optimization algorithm for hyperparameter tuning. The proposed antenna obtained return loss values of -36.01 dB and -39 dB at the resonating frequencies of 5.64 GHz and 5.73 GHz, respectively. It achieved gain values of 12.41 dB, 10.7 dB, and ECC values of less than 0.025. The proposed model obtained better results than other models in this comparison analysis.

1. INTRODUCTION

Wireless communication systems heavily rely on satellite transmission to meet the increasing demand for fast data throughput [1]. To address this demand, numerous approaches have been developed to enhance data rates in wireless communication systems [2]. These approaches include advanced technologies such as MIMO technologies [3], orthogonal frequency division multiplexing (OFDM) [4], carrier aggregation (CA) [5], beamforming, hybrid automatic repeat request (HARQ) [6], spectrum sharing [7], dynamic spectrum access [8], and advanced modulation schemes [9].

MIMO antennas are widely used for their ability to transmit and receive multiple data streams simultaneously, thereby increasing data throughput and spectral efficiency [10]. However, the design and implementation of MIMO antennas pose several challenges, particularly due to the small distances between antenna elements [11]. One of the main challenges is achieving desired radiation characteristics and operational efficiency within limited physical dimensions. This is because the small distances between antenna elements can result in mutual coupling, which can degrade the performance of the MIMO system [12]. Mutual coupling is the interference between adjacent antennas, which can lead to a decrease in signal quality and an increase in signal correlation. This can result in a decrease in diversity gain, which is the ability of the MIMO system to exploit multiple spatial paths to improve signal quality [13]. For

example, in a four-port MIMO system, if the correlation between the antennas is high, the system may only be able to exploit two spatial paths effectively, resulting in reduced diversity gain compared to a system with a lower correlation [14]. Another challenge is achieving operational efficiency within limited physical dimensions. This is because the small distances between antenna elements can result in a decrease in isolation, which is the ability of the antennas to reject interference from other antennas [15]. This can lead to a decrease in signal quality and an increase in power consumption. For example, in a four-port MIMO system, if the isolation between the antennas is low, the system may require more power to achieve the same signal quality than a system with higher isolation [16]. To overcome these challenges, several strategies are employed. Antenna decoupling is a technique used to reduce the mutual coupling between antennas. This can be achieved through various methods, such as decoupling structures, absorber walls, and parasitic elements. Diversity schemes are used to improve the diversity gain of the MIMO system [17, 18]. This can be achieved through various methods, such as spatial diversity, polarization diversity, and frequency diversity [19]. Advanced array configurations are used to improve the isolation and operational efficiency of the MIMO system. This can be achieved through various methods, such as using beamforming, null steering, and frequency reconfigurability [20].

Frequency reconfiguration technologies, including PIN diodes, reactors, radio-frequency microelectromechanical systems (RF-MEMS), and diodes, play a crucial role in achieving

* Corresponding author: Maruti R. Jadhav (maruti.jadhavdte@gmail.com).

efficient and compact frequency reconfiguration for MIMO antennas [21]. PIN diodes are useful for frequency reconfiguration due to their ability to change impedance quickly and efficiently [22]. Reactors consist of a series of inductors and capacitors that can be tuned to change the impedance of the antenna [23]. radio frequency micro-electromechanical system (RF-MEMS) devices can be used to change the impedance of an antenna by adjusting the size or shape of the device [24]. Diodes can be used to change the impedance of an antenna by changing the phase of the current flowing through the diode [25]. These technologies enable rapid changes in impedance, allowing for dynamic adjustment of antenna parameters to suit varying operating conditions. In the context of small wireless devices and vehicle-to-everything (V2X) systems, the development of compact, frequency-configurable MIMO antennas is essential for practical applications [26]. Frequency reconfiguration involves electronically adjusting the radiator's length, necessitating switching electronics to change the operating frequency bands [27]. While PIN-based reconfiguration offers advantages such as short response latency and compact implementation, integrating PIN diodes into MIMO antennas may lead to overall enlargement of the antenna [28].

The evolution of cellular networks, particularly with the advent of 5G technology, has further propelled the demand for advanced MIMO antenna designs [29]. In 5G-enabled devices, MIMO antennas are crucial for transmitting data at high speeds with variable patterns, spatial distribution, and polarization over a wide frequency range [30]. However, integrating MIMO components into smartphones poses challenges due to limitations in isolation and efficiency [31].

In V2X applications, MIMO array antennas are used to generate linear polarization (LP) radiation for LTE and ultra-wideband (UWB) applications [32]. Diverse linearly polarised broadband MIMO diversity antennas have been implemented in wireless applications, achieving isolation greater than >17 dB. [33]. Cellular networks are widely considered the backbone of V2X connection technology, especially C-V2X, in terms of reducing traffic accidents. These cellular networks are being modernized to speed up communication. Some V2X applications use the 5G network, which operates at millimeter wave and sub-6 GHz frequencies [34]. Finally, the proposed research seeks to advance existing MIMO antenna designs and facilitate the integration of MIMO components into small wireless devices and V2X systems. By leveraging frequency reconfiguration technologies and addressing the challenges in antenna design, the research aims to improve the performance of MIMO systems and V2X communication.

1.1. Motivation

The motivation for the proposed antenna design is to address the identified challenges in existing MIMO antenna models for dual-band applications. The current models have several disadvantages, including insufficient isolation, low mutual coupling, and low reliability. These issues can lead to performance degradation and reduced efficiency in MIMO systems. To overcome these challenges, a novel eight-port EBG resonator MIMO antenna is proposed. The proposed design incorporates an EBG

resonator structure, which has been shown to improve isolation and reliability while reducing polarization effects in MIMO antennas. By addressing these challenges, the proposed antenna design aims to enhance the performance of dual-band MIMO systems in wireless communication applications. The following sections contribute to the development of the proposed antenna design.

- To present an eight-port MIMO antenna and an EBG resonator for V2X applications.
- To introduce an EBG resonator to enhance isolation and overcome mutual coupling issues.
- To present a plus shape DGS on a polyamide substrate to increase efficiency and reduce polarization loss.
- By using the BWP optimization method, the proposed 8-port MIMO antenna design can achieve optimal values for the design parameters, leading to improved gain, return loss, and efficiency.
- A number of the suggested design's performance metrics are examined to enhance the MIMO antenna's efficacy and performance.

The proposed research work on MIMO antennas is organized into five sections. The introduction section provides an overview of the research work, including the motivation and objectives of the study. It highlights the challenges in existing MIMO antenna models, such as insufficient isolation, low mutual coupling, and low reliability, and proposes a solution using an 8-port EBG resonator MIMO antenna. The section concludes with the organization of the paper. Section 2 presents a comprehensive review of the state-of-the-art research on MIMO antennas, including their design, advantages, and limitations. It discusses the challenges faced in MIMO antenna design and concludes with the need for a novel MIMO antenna design that addresses these challenges. Section 3 describes the proposed 8-port EBG resonator MIMO antenna design, including the design parameters and optimization method. It presents the design methodology, simulation setup, and results and compares the proposed design with existing models, highlighting the advantages and improvements achieved. Section 4 provides a detailed analysis of the proposed MIMO antenna design's performance, including isolation, mutual coupling, and reliability. It compares the proposed design with existing models, highlights the improvements achieved, and discusses the potential applications and future directions for the proposed design. Section 5 summarizes the research work, highlighting the contributions and achievements. It discusses the implications of the proposed design for MIMO antenna design and wireless communication systems and concludes with the limitations of the study and potential directions for future research.

2. RELATED WORKS

Some of the latest research tasks correlated to MIMO antenna design for V2X applications are surveyed below:

Fu et al. [35] designed a two port-MIMO antenna for V2X communication. This antenna aims to reduce the coupling of antenna elements. The frequency is between 3.8 and 4.8 GHz

employed in this antenna. It uses comb line filters and absorption wall decoupling in two ways. The absorption unit size of the absorber wall is only $13 \times 13 \text{ mm}^2$, and the coupling of the MIMO antenna is reduced by a combine filter and absorption wall. The decrease in mutual coupling between adjacent antennas is elucidated in this study through the utilization of absorber walls in conjunction with an electromagnetic field distribution technique. The antenna consists of a two-layer substrate connected by a coaxial feed. Substrates 1 and 2 adopt the Ro4003 material with a thickness of $h = 1.524 \text{ mm}$ and the FR-4 material with a thickness of $h = 1.5 \text{ mm}$. Evaluation of the antenna's performance includes assessing bandwidth, peak gain, and the ECC. The limitation of two port-MIMO antennae for V2X communication is obtained by limited diversity gain. With only two ports, the antenna may not be able to exploit multiple spatial paths effectively, resulting in reduced diversity gain compared to antennas with more ports.

Ez-Zaki et al. [36] devised a novel approach to address mutual coupling issues in DSRC/sub-6 GHz Koch fractal antennas. Their design encompasses single, two, and four-element configurations integrated with metamaterial structures to enhance diversity performance. The primary focus is on mitigating mutual coupling among MIMO antenna ports. The antenna elements are printed on a 1.6 mm thick FR-4 substrate with a permittivity of $\epsilon_r = 4.4$, operating at 5.9 GHz for DSRC and C-V2X communication. The installation of two new double negative (DNG) metamaterial structures on either side of the substrate helps to reduce mutual coupling while enhancing diversity performance. Reflection coefficients, isolation, and diversity performance indicators such as ECC, DG, MEG, TARC, and channel capacity loss (CCL) are evaluated for single, two, and four-element antennas. DSRC/sub-6 GHz Koch fractal antennas have the disadvantage of being difficult to design and fabricate.

Chung et al. [37] designed a three-element circularly polarized MIMO (CP-MIMO) antenna array employing a self-decoupled method. This designed antenna aimed to improve high data throughput and enhanced channel capacity at high spectral efficiencies. The antenna comprises Guo-character-shaped patch elements designed for B5G-V2X applications. Three unidirectional radiated Guo-shaped patch antennas were assembled in a triangular lattice and activated by L-shaped feeding probes placed at varying angles to the patch center. This approach, positioned as a strong candidate in multi-user B5G-V2X scenarios, allows polarization variety, spatial diversity, and pattern variation while providing better isolation (25 dB) between patch pieces without the need for an external decoupling mechanism. This recommended CP-MIMO antenna, which operates at 2.4 to 2.5 GHz, was thoroughly tested for MIMO performance metrics such as ECC, MEG, CCL, TARC, and spatial multiplexing efficiency. The disadvantage of a CP-MIMO antenna array that uses a self-decoupled technique is the possibility of higher design and implementation complexity.

Aliqab et al. [38] designed a novel approach to address mutual coupling in MIMO antennas, focusing on simplicity, cost-effectiveness, and compactness. The antenna operates in the

automotive communications frequency band of 5.85 GHz to 5.95 GHz. It consists of two separate radiating components, each with slits to improve isolation between the radiators. The MIMO antenna, intended for vehicular-to-everything (V2X) applications, has small dimensions and is printed on a 0.6 mm flexible polyimide substrate. A significant result of the investigation was a surprisingly low isolation level of 28 dB across the full operational range. The suggested configuration is analyzed using S parameters, radiation characteristics, efficiency, gain, and diversity performance measures like ECC, DG, and TARC. This antenna's limitations cause issues in terms of diversity gain, interference, beamforming, and channel correlation.

Rakluea et al. [39] designed an efficient method involving the development of a triple-port ultra-wideband (UWB) MIMO antenna tailored for wireless communication applications. The primary objective of this antenna design was to create a versatile antenna capable of conforming to various surfaces, including automobile glass, to simplify installation procedures. To achieve this, the antenna employed a substrate made of carbon-black window film. Additionally, the automotive film is coated with a conductive substance comprising copper tape, characterized by a thickness of 0.07 mm and a conductivity (σ) value of $5.8 \times 10^7 \text{ S}$. The antenna has a wide frequency range, ranging from 3.1 GHz to 10.6 GHz over three ports. This broad frequency range allows for the possible support of a variety of wireless communication technologies, including wireless personal area networks (WPAN), UWB, 5G, WiMAX, and WLAN. The antenna's performance is evaluated based on bandwidth, peak gain, and ECC. A triple-port UWB MIMO antenna designed for wireless communication applications may have drawbacks such as complexity and cost.

Wong et al. [40] developed a compact 8-port MIMO antenna module and its 1×2 array for 6G 16×8 device MIMO applications. They aimed to achieve high isolation, efficiency, low envelope correlation coefficient, and diversity gain for these applications. The design achieves 30 dB isolation, over 80% efficiency, and a compact size of $0.16\lambda_0 \times 0.16\lambda_0$. It also maintains a low ECC of less than 0.05 and a diversity gain of over 9.5 dB. The design consists of eight folded monopole antennas and a parasitic strip, printed on a Rogers RO4003C substrate. Operating at a center frequency of 28 GHz, it covers the entire 6G frequency band of 24.25–29.5 GHz. Additionally, a 1×2 array is included, formed by combining two 8-port MIMO antenna modules, achieving 25 dB isolation, over 80% efficiency, and a compact size of $0.32\lambda_0 \times 0.16\lambda_0$. While suitable for 6G devices like smartphones, tablets, and laptops, the limitation of this design is its compatibility only within the 6G frequency band of 24.25–29.5 GHz.

Sufyan et al. [41] devised a dual-band, independently tunable 8-element MIMO antenna tailored for 5G smartphones, with a focus on achieving dual-band operation and high isolation between adjacent antennas in 5G MIMO scenarios. The antenna boasts impressive features, including a 20 dB isolation, over 70% efficiency, and a compact size of $0.1\lambda_0 \times 0.1\lambda_0$. Constructed from eight folded monopole antennas and a tuning network, printed on a Rogers RO4003C substrate, the antenna operates at two center frequencies, covering the entire 5G

frequency band of 3.3–3.8 GHz and 24.25–29.5 GHz. Additionally, it incorporates a tuning network to adjust antenna elements' resonant frequency, achieving a low ECC of less than 0.05 and a diversity gain exceeding 9.5 dB. Although suitable for 5G smartphones requiring dual-band operation and high isolation, the design complexity and cost are heightened by the use of PIN diodes.

Guo et al. [42] devised an innovative combined open-slot and monopole 8×8 high-isolation broadband MIMO antenna system tailored for sub-6 GHz terminals. Their primary aim was to achieve exceptional isolation, efficiency, and broad bandwidth for sub-6 GHz MIMO applications. Remarkably, the designed antenna achieves a 25 dB isolation, over 80% efficiency, and compact dimensions of $0.2\lambda_0 \times 0.2\lambda_0$. Constructed from eight open-slot antennas and eight monopole antennas, printed on a Rogers RO4003C substrate, the antenna operates at a center frequency of 3.5 GHz, covering the entire sub-6 GHz frequency band of 3.3–4.2 GHz. It achieves a low ECC of less than 0.05 and a diversity gain exceeding 9.5 dB. This design is well-suited for sub-6 GHz terminals like smartphones, tablets, and laptops. However, it's limited to the sub-6 GHz band and may not be suitable for other frequencies or applications.

Khan et al. [43] developed a dual-band 8×8 MIMO antenna system tailored for 5G smartphones, functioning at 3.5 GHz and 5.5 GHz. The goal was to showcase its applicability in 5G smartphone technology. The designed antenna setup comprises 64 elements, each featuring a modified F-shaped radiator positioned on the smartphone's PCB edge. The radiator dimensions are $140 \times 70 \text{ mm}^2$, while each element measures $4.5 \times 11 \text{ mm}^2$ ($0.05\lambda \times 0.16\lambda$). To enhance isolation between elements, two isolator types were utilized: a defected ground structure for close elements and T- and L-shaped isolators for distant ones. Mutual couplings below -20 dB and -22 dB were achieved in the lower and higher bands, respectively. The envelope correlation coefficient among elements is < 0.11 , with radiation efficiencies exceeding 68% and 78% in the lower and higher bands, respectively. However, the high manufacturing costs remain a concern. Table 1 presents an overview of the existing MIMO antenna designs.

In recent years, communication technologies based on V2X have been developed using MIMO systems. This technology allows signal propagation to be controlled electronically, which makes it possible to send and receive signals using multiple antennas. This means that data can be transferred and received more efficiently without requiring additional capacity. However, when the antennas are too close together, they can interfere with each other, which can cause problems with the data transfer. To solve this issue, researchers are developing MIMO antennas with very low interference. Several techniques are being used to try to reduce this interference, an important area of research in academia and industry. Various types of mutual coupling reduction techniques have been reported in the literature [35–43]. However, existing MIMO designs encounter several challenges, including limited diversity gain [35], complexities in design-to-fabrication processes [36], high design and implementation complexity [37], as well as difficulties in addressing diversity gain, interference, beamforming, and polarization

correlation [38]. Additionally, concerns regarding high complexity and cost-effectiveness [39], model complexity [40, 41], decreased efficiency [42], and high manufacturing costs [43] persist. To overcome these issues, and reduce mutual coupling, a novel dual-band 8-port MIMO antenna based on metamaterial is being developed for V2X applications.

3. PROPOSED GEOMETRY

Communication systems frequently employ MIMO antennas to transmit and receive data signals with minimal latency. For V2X applications, a novel dual-band 8-port MIMO antenna based on metamaterial is being developed. The proposed antenna has less polarization effects and is more reliable than other antenna designs. Two frequencies ranging from 5.6 to 5.8 GHz are utilized for band gap electromagnetic resonance IoT applications in an eight-port MIMO antenna. To enhance isolation, the MIMO antenna is constructed on a polyimide substrate and employs a CWF. This investigation employs a flawed ground construction to minimize the interfering signals between the antennas. The dimensions of the proposed antenna are $80 \times 80 \times 0.1 \text{ mm}$, indicating miniaturization. The antenna design is developed, simulated, and analyzed by HFSS software.

The initial stage in designing an antenna is to select the correct dielectric substrate. Here, the substrate used is polyimide, with a thickness of 0.1 mm, permittivity of 3.5, and loss tangent of 0.008, which is highly flexible and robust. The antenna is designed to feed with CPW on the substrate. In this work, the length and width of an antenna are computed using the following equations:

The width (V) of the antenna is computed by:

$$V = \frac{r_0}{2C_x} \sqrt{\frac{2}{\epsilon_x + 1}} \quad (1)$$

Here, C_x is denoted as the resonant frequency, r_0 denoted as the velocity, and ϵ_x denoted as the dielectric constant. The effective ϵ_x is represented as:

$$\epsilon_{\text{reff}} = \frac{\epsilon_x + 1}{2} + \frac{\epsilon_x - 1}{2} \left[1 + \frac{10U}{V} \right] \quad (2)$$

Here, U is denoted as the ϵ_x dielectric substrate's height, and the effective length (H_{eff}) is given as:

$$H_{\text{eff}} = \frac{r_0}{2C_x \sqrt{\epsilon_{\text{reff}}}} \quad (3)$$

The actual antenna length (H) is given as follows:

$$H = H_{\text{eff}} - 2\Delta H \quad (4)$$

Here, ΔH is denoted as the extension length, which is calculated using the below formula:

$$\Delta H = 0.412 \times U \times \frac{(\epsilon_x + 0.3) \left(\frac{V}{U} + 0.26 \right)}{(\epsilon_x - 0.253) \left(\frac{V}{U} + 0.8 \right)} \quad (5)$$

TABLE 1. A summary of existing MIMO works.

Authors and Refer	Design	Applications	Objective	Strengths	Weaknesses	Performance
Fu et al. [35]	Two-port MIMO	V2X communication	To reduce the coupling of antenna elements	Reduced coupling between antenna elements, wide bandwidth	Limited diversity gain, relatively low resonant frequency	Bandwidth, peak gain, and the ECC
Ez-Zaki et al. [36]	4-port MIMO	Wireless communication	To enhance diversity performance	Reduce mutual coupling and enhance diversity performance	Design to fabrication complexity	Reflection coefficients, isolation, and diversity performance metrics such as ECC, DG, MEG, TARC, and CCL
Chung et al. [37]	3 port CP-MIMO	B5G-V2x communication	To improve high data throughput and enhanced channel capacity at high spectral efficiencies	Reduce mutual coupling and enhance diversity performance	High design and implementation complexity	ECC, MEG, CCL, TARC, and spatial multiplexing efficiency
Aliqab et al. [38]	2-port MIMO	Vehicular communications	To reduce simplicity, cost-effectiveness, and compactness.	Higher diversity gain, interference reduction, beamforming, and channel correlation	Challenges related to diversity gain, interference, beamforming, and channel correlation	<i>S</i> parameters, radiation characteristics, efficiency, gain, and diversity performance metrics such as ECC, DG, and TARC
Raklua et al. [39]	3-port UWB- MIMO	UWB ,WiMAX, and WPAN	To create a versatile antenna capable of conforming to various surfaces, including automobile glass, to simplify installation procedures	Higher isolation and reduced mutual coupling between antenna elements	High complexity and High cost-effectiveness	Bandwidth, peak gain, and the ECC
Wong et al. [40]	8-port MIMO	6G Application	To achieve high isolation, efficiency, low envelope correlation coefficient, and diversity gain for these applications	To achieve high isolation, high efficiency, and compact size.	Compatibility only within the 6G frequency band of 24.25–29.5 GHz	<i>S</i> parameters, radiation characteristics, efficiency, gain, and diversity performance metrics such as ECC, DG, and TARC
Sufyan et al. [41]	8-port MIMO	Suitable for 5G smartphones.	To achieve dual-band operation and high isolation between adjacent antennas in 5G MIMO scenarios	To independently tunable frequency bands using PIN diodes.	increase the complexity and cost of the design	Bandwidth, peak gain, and the ECC,DG
Guo et al. [42]	8-port MIMO	Sub-6 GHz terminals	To achieve high isolation, high efficiency, and broad band width for sub-6 GHz MIMO applications	The antenna uses a combination of open-slot and monopole antennas to achieve high isolation and broad bandwidth	Not be suitable for other frequency bands or applications	ECC, DG, MEG, TARC, and CCL
Khan et al. [43]	8-port MIMO	5G smartphone applications	To enhance isolation	To provide high-isolation	high manufacturing costs	ECC, DG, MEG, TARC, and CCL

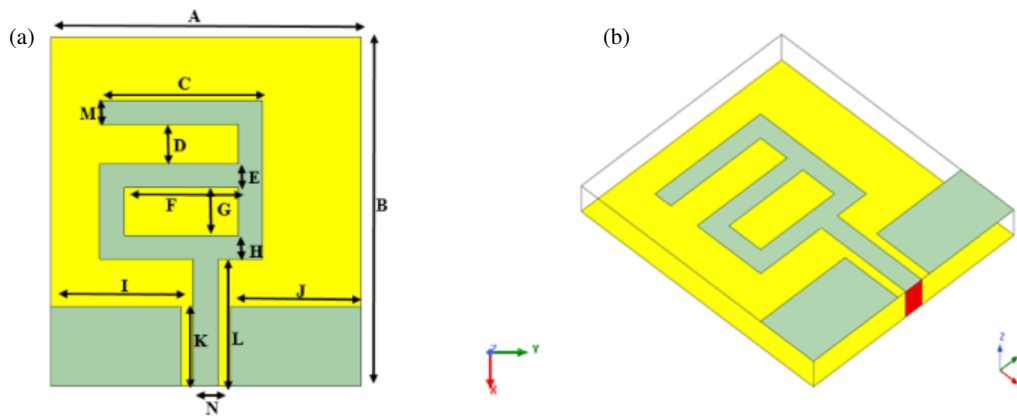


FIGURE 1. 2D and 3D view of Single port antenna design.

The feed line's length (H_f) is represented as:

$$H_f = \frac{\lambda_k}{4} \tag{6}$$

Here, λ_k is denoted as the guided wavelength.

3.1. Single Port MIMO Antenna Design

The “a” designed antenna construction with a DGS is used to achieve resonance in the desired frequency ranges of 5.6 to 5.8 GHz. The “a” structure may accommodate two independent present paths, allowing the single monopole antenna to achieve dual-band resonance. The CPW feed line is displaced from the centre of the ‘a’-shaped structure in order to accommodate the 2.7 GHz and 3.65 GHz centre frequencies of the monopole antenna construction. The DGS improves the impedance matching of monopole antennas. The HFSS platform is utilized to optimise the dimensions of individual antenna design parameters via simulation. The development of a single port [44] MIMO antenna is illustrated in 2D and 3D views, respectively, in Figures 1(a) and 1(b). Table 2 indicates the measurements of a single port MIMO antenna.

TABLE 2. Measurements of the single-port MIMO antenna.

Dimensions	Specifications	Dimensions	Specifications
<i>A</i>	19 mm	<i>H</i>	1.5 mm
<i>B</i>	22 mm	<i>I</i>	8 mm
<i>C</i>	10 mm	<i>J</i>	8 mm
<i>D</i>	2.5 mm	<i>K</i>	5 mm
<i>E</i>	1.5 mm	<i>L</i>	8 mm
<i>F</i>	7 mm	<i>M</i>	1.5 mm
<i>G</i>	3 mm	<i>N</i>	1.5 mm

Figure 1(a) illustrates a two-dimensional representation of a single-port antenna configuration incorporating a DGS ground antenna. A three-dimensional representation of a single-port antenna configuration comprising a CPW feed line and DGS ground is illustrated in Figure 1(b).

3.2. Two-Port MIMO Antenna Design

Prior to constructing the two-port antenna [45], the two individual antenna components are affixed to a polyimide substrate at a consistent distance of 18.5 mm between each element of the antenna. The isolation at two centre frequencies, namely 3.68 GHz and 2.5 GHz, is inadequate. The intense mutual contact between the antenna components and the ground plane hinders optimal operation, despite the antenna's diminutive size. After port 1 is operational and port 2 is terminated with a matched load, the surface current distribution at 2.5 GHz and 3.68 GHz reveals substantial mutual coupling on the antenna element that remains close to the ground plane. Figures 2(a) and 2(b) show the two-port MIMO antennas in 2D and 3D designs, which are also integrated into the recommended antenna design. Table 3 indicates the measurements of a two-port MIMO antenna.

TABLE 3. Measurements of the two-port MIMO antenna.

Dimensions	Specifications	Dimensions	Specifications
<i>A</i>	44 mm	<i>N</i>	8 mm
<i>B</i>	22 mm	<i>O</i>	1.5 mm
<i>C</i>	10 mm	<i>P</i>	8 mm
<i>D</i>	2.5 mm	<i>Q</i>	5 mm
<i>E</i>	6 mm	<i>R</i>	1.5 mm
<i>F</i>	1.5 mm	<i>S</i>	2.5 mm
<i>G</i>	1.5 mm	<i>T</i>	3 mm
<i>H</i>	3 mm	<i>U</i>	1.5 mm
<i>I</i>	1.5 mm	<i>V</i>	8 mm
<i>J</i>	10 mm	<i>W</i>	1 mm
<i>K</i>	1 mm	<i>X</i>	8 mm
<i>L</i>	8 mm	<i>Y</i>	5 mm
<i>M</i>	5 mm	<i>Z</i>	1.5 mm

A two-dimensional view of a two-port MIMO antenna featuring a DGS ground antenna is illustrated in Figure 2(a). 3D representation of a two-port MIMO antenna configuration featuring a CPW feed line and DGS ground is illustrated in Figure 2(b).

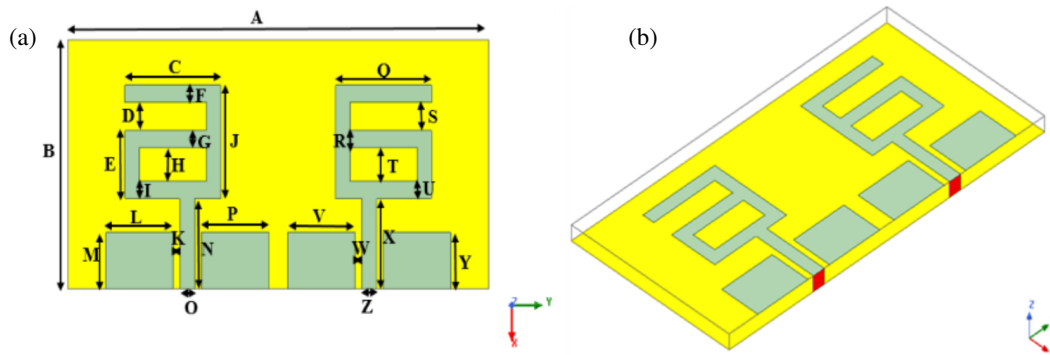


FIGURE 2. 2D and 3D design of two port MIMO antenna.

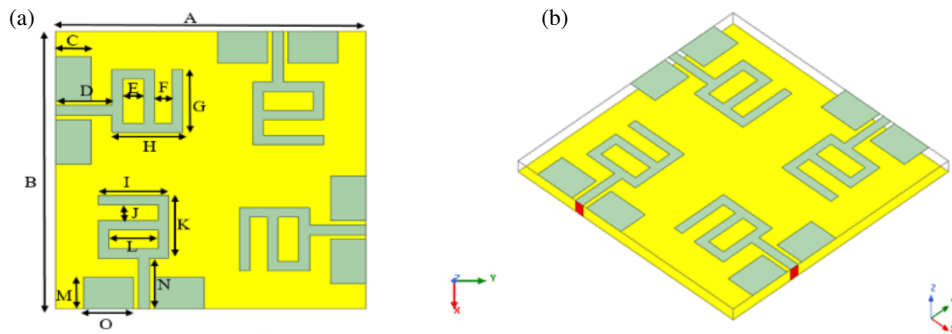


FIGURE 3. 2D and 3D design of four port MIMO antenna.

3.3. Four-port MIMO Antenna Design

The antenna development proposal also incorporates provisions for a four-port MIMO antenna [46]. As illustrated in Figures 3(a) and 3(b), the four-port MIMO antennas' 2D and 3D designs are corresponding to the figures. Table 4 indicates the measurements of a four-port MIMO antenna.

TABLE 4. Measurements of the four-port MIMO antenna.

Dimensions	Specifications	Dimensions	Specifications
<i>A</i>	44 mm	<i>I</i>	10 mm
<i>B</i>	44 mm	<i>J</i>	2.5 mm
<i>C</i>	5 mm	<i>K</i>	10 mm
<i>D</i>	8 mm	<i>L</i>	7 mm
<i>E</i>	3 mm	<i>M</i>	5 mm
<i>F</i>	2.5 mm	<i>N</i>	8 mm
<i>G</i>	10 mm	<i>O</i>	8 mm
<i>H</i>	10 mm		

Figure 3(a) illustrates the two-dimensional representation of a four-port MIMO antenna configuration featuring a DGS ground and tower. A three-dimensional illustration of a four-port MIMO antenna configuration featuring a CPW feed line and DGS ground is illustrated in Figure 3(b).

3.4. Proposed Eight-Port MIMO Antenna Design

The proposed antenna development is also designed for an 8-port MIMO antenna. It consists of a plus-shape DGS and EBG

metamaterial as well as a polyimide substrate and a CPW feed-line for high isolation. The proposed eight-port MIMO antenna design is illustrated in Figure 4. The 2D and 3D configurations of the eight-port MIMO antenna are presented in Figures 5(a) and 5(b), respectively.

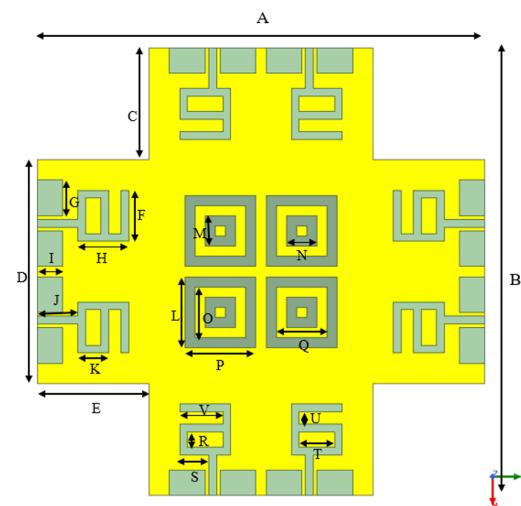


FIGURE 4. Design of proposed eight-port MIMO antenna.

Figure 5(a) shows a 2D representation of an 8-port MIMO antenna design combined with a plus-shape DGS ground antenna. A proposed eight-port MIMO antenna design, including a plus-form DGS ground, a CPW matching circuit, and an antenna, is depicted in three dimensions in Figure 5(b). The figure also shows an EBG metamaterial design.

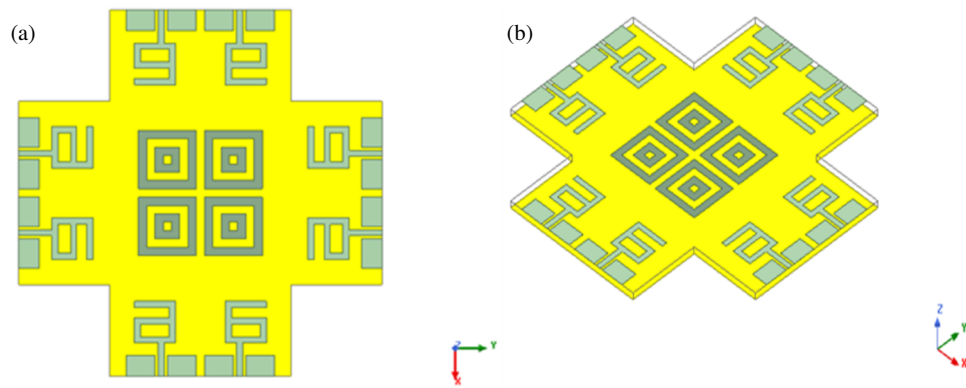


FIGURE 5. 2D and 3D design of eight port MIMO antenna.

3.5. Proposed MIMO Antenna Consolidated with Plus Shape DGS and EBG Metamaterial

The combination of EBG metamaterials and plus-shaped DGS in the proposed MIMO antenna design allows for improved isolation, mutual coupling, and reliability, making it well-suited for V2X applications. The EBG metamaterial produces electromagnetic signals that facilitate radio wave transmission for reliable communication, while the plus-shaped DGS minimizes the size of the antenna and reduces mutual coupling. The resulting MIMO antenna is compact, efficient, and reliable, making it a promising candidate for V2X communications in the 5.6GHz–5.8GHz frequency range.

In the proposed MIMO antenna development, a plus-shaped DGS minimizes the mutual coupling values for successful communication. The antennas have a high level of mutual contact. In general, DGS can determine the degree of coupling between nearby MIMO antennas. The baseplate comprises a bonded copper layer that underpins the proposed DGS structure, which is comprised of four boomerang-shaped segments connected to the larger ring and two circular rings arranged in its center. As the frequency increases, the proposed DGS diminishes the value of coupling between adjacent antennas. MIMO communication performance is typically degraded by excessive mutual coupling; therefore, the DGS structure is implemented to reduce mutual coupling. The performance of the proposed MIMO antenna is improved by reducing the coupling value.

The metamaterial EBG resonator in the proposed MIMO architecture is located in the middle of the eight ports of the antenna. The EBG arrangement is examined to determine the impact of reducing the array size. The metamaterial-based EBG structure is designed and integrated into the antenna to improve radiation efficiency and reduce SAR. The EBG metamaterial generates electromagnetic signals that help transmit radio waves during communication. The proposed total size of the EBG is 14 mm × 14 mm. The inner and outer rings of the proposed EBG structure are composed of double ring rectangles.

This EBG runs between 5.6 and 5.8 GHz. By modifying the parameter values 14, 16, and 10, the outer ring's size of 14 mm, which responds to the dual-band resonance at 5.6 GHz, can be modified. The EBG runs at a different frequency when the in-

ner ring is added. The inner ring has a diameter of 10 mm and works at 5.8 GHz. The inner ring's inclusion does not influence the 2.4 GHz band. This indicates that modifications to one of the two rings have minimal impact on the other. As a result, the operating frequencies can be adjusted by changing the size of each ring individually. Figure 6 displays the design of the Metamaterial EBG resonator, and Figures 7(a) and 7(b) depict the 2D and 3D designs of the EBG resonators.

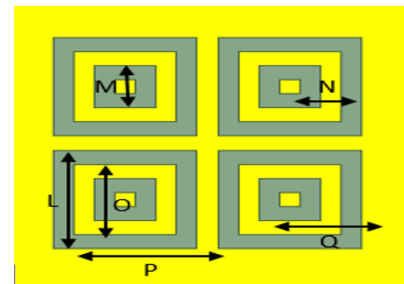


FIGURE 6. EBG resonator.

The metamaterial is also used to provide magnetic and electrical boundary conditions. A rectangular material is defined on the floor structure between the antennas. By integrating EBG metamaterials into the MIMO antenna design, it is possible to achieve improved isolation, mutual coupling, and reliability compared to existing models. The proposed 8-port MIMO antenna simulation parameters and criteria used in the HFSS platform are shown in Table 5.

The proposed metamaterial EBG resonator is combined with an 8-port dual-band MIMO antenna and uses the characteristics listed in Table 6. This resonator supports effective electromagnetic signals that increase the transmission rate. Figure 8 shows the fabricated design of the proposed 8-port dual-band MIMO antenna.

3.6. Parameter Optimization of MIMO Antenna Using BWP

Optimization algorithms are tools that help improve the performance and efficiency of antennas. Some of the commonly used algorithms include Genetic Algorithm (GA), Particle Swarm Optimization (PSO), Simulated Annealing (SA), Ant Colony

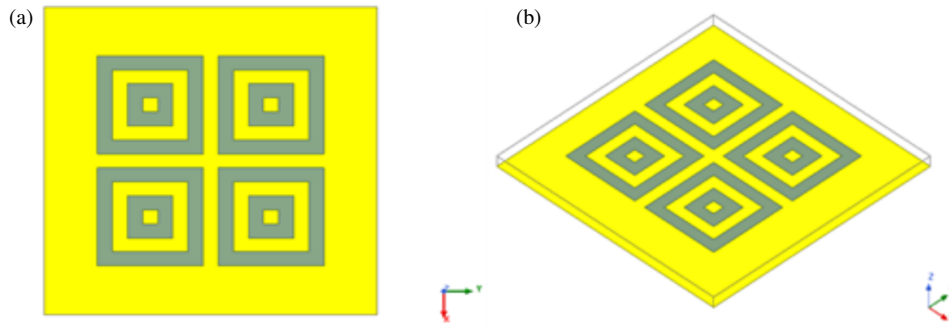


FIGURE 7. 2D and 3D design of the EBG resonator.

TABLE 5. Dimensions and specifications of the proposed 8-port MIMO antenna.

Dimensions	Specifications	Dimensions	Specifications
<i>A</i>	88 mm	<i>L</i>	14 mm
<i>B</i>	88 mm	<i>M</i>	6 mm
<i>C</i>	22 mm	<i>N</i>	6 mm
<i>D</i>	44 mm	<i>O</i>	10 mm
<i>E</i>	22 mm	<i>P</i>	14 mm
<i>F</i>	10 mm	<i>Q</i>	10 mm
<i>G</i>	7 mm	<i>R</i>	3 mm
<i>H</i>	10 mm	<i>S</i>	5.75 mm
<i>I</i>	5 mm	<i>T</i>	7 mm
<i>J</i>	8 mm	<i>U</i>	2.5 mm
<i>K</i>	6 mm	<i>V</i>	8.5 mm

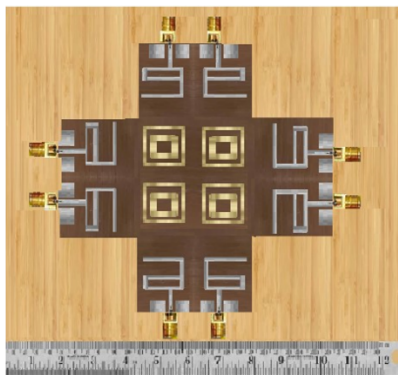


FIGURE 8. 8-port MIMO antenna fabricated design.

Optimization (ACO), and Cuckoo Search (CS). While GA and PSO have some limitations, such as struggling to explore all possibilities and being sensitive to their settings, SA, ACO, and CS are more effective at exploring the search space. In this research, we utilized a novel algorithm called BWP, inspired by the waterwheel plant, which traps prey like a Venus flytrap. This algorithm is used to enhance the performance of an 8-port MIMO antenna model. By adjusting antenna parameters such as length, height, and substrate material, the BWP optimization algorithm improves the gain of the antenna. The effective

tuning capability of the BWP optimization algorithm enhances the antenna’s performance across different measures, resulting in better gain, reduced signal loss, and higher efficiency. By using BWP to fine-tune the antenna design, we were able to significantly improve its performance, demonstrating the effectiveness of this novel approach.

3.6.1. Initialization

The waterwheel plant algorithm is a population-based technique that delivers an appropriate solution based on the search power of its population members in the universe of possible solutions to the problem. It initializes the positions of waterwheels, which represent possible solutions to the problem, randomly at the outset of WWPA implementation. Each waterwheel is mathematically represented by a vector, and the WWPA population, which includes all the waterwheels, may be represented by a matrix (7). The waterwheels’ positions in the search space are randomly initialized at the outset of WWPA implementation using (8)

$$G = \begin{bmatrix} G_1 \\ \vdots \\ G_p \\ \vdots \\ G_m \end{bmatrix}_{m \times n} = \begin{bmatrix} g_{1,1} & \cdots & g_{1,q} & \cdots & g_{1,n} \\ \vdots & \ddots & \vdots & \ddots & \vdots \\ g_{p,1} & \cdots & g_{p,q} & \cdots & g_{p,n} \\ \vdots & \ddots & \vdots & \ddots & \vdots \\ g_{m,1} & \cdots & g_{m,q} & \cdots & g_{m,n} \end{bmatrix}_{m \times n} \quad (7)$$

$$G_{p,q} = mk_q + f_{p,q}(hk_q - mk_q), \quad p = 1, 2, \dots, N, \quad q = 1, 2, \dots, M \quad (8)$$

Here, the number of waterwheels and the number of variables are denoted by N and m , respectively; $f_{p,q}$ is denoted as a random number in the interval $[0, 1]$; the lower bound and upper bound of the q -th problem variable are denoted as the mk_q and hk_q . The population matrix of waterwheel locations is denoted as the G ; G_p denotes the p -th waterwheel; and $G_{p,q}$ is denoted as the p th and q th waterwheel location.

Each antenna element represents a potential solution to the problem, so the objective function can be calculated for each. It has been shown that a vector may be used to effectively represent the values that have been determined to constitute the

TABLE 6. Step-by-step description of the algorithm used to design the dual band MIMO antenna.

Algorithm: To Design, Analyze, and Model 5.6 and 5.8 GHz Dual Band MIMO to enhance Gain for V2X application
Input: Specification and dimension Table 2, frequency 5.6 GHz to 5.8 GHz, Dual-band, 8-port.
Output : Gain, VSWR , and ECC
Step 1: Metamaterial Selection: The proposed antenna Chooses EBG metamaterials, its center of antenna and total size of 14 mm×14 mm.
Step 2: CPW Design: The CPW feed line is placed in the eight-port 'a'-shaped structure.
Step 3: Frequency Band Selection: The proposed eight-port MIMO antenna can be selected a frequency range of 5.6 GHz to 5.8 GHz.
Step 4: Substrate Material Selection: The proposed antenna-selected polyimide substrate for better performance of the antenna.
Step 5: DGS Implementation: Integrate plus-shaped DGS to the antenna design to reduce mutual coupling between antenna elements.
Step 6: Optimization Technique: Binary Waterwheel Plant (BWP) to optimize design parameters, ensuring optimal performance across key metrics.
Step 7: Simulation and Analysis: Simulate the designed MIMO antenna using HFSS simulation software to analyze performance metrics like bandwidth, gain, return loss radiation pattern, isolation, DG, TARC, VSWR, and ECC.

objective function of the problem (9)

$$F = \begin{bmatrix} F_1 \\ \vdots \\ F_p \\ \vdots \\ F_m \end{bmatrix}_{m \times 1} = \begin{bmatrix} F(G_1) \\ \vdots \\ F(G_p) \\ \vdots \\ F(G_m) \end{bmatrix}_{m \times 1} \quad (9)$$

where F is the vector of all the objective function values, and F_p is the estimated value for the p th antenna element. The objective function evaluations are the key metrics for selecting the best solutions. The best candidate solution corresponds to the highest value of the objective function, and the lowest value corresponds to the worst candidate solution. The algorithm's iterative optimization process ensures robustness and reliability. The flexibility of the BWP algorithm allows it to be adapted for different antenna design problems.

3.6.2. Exploration: Location Identification and Best Solution for Antenna Design

The antenna exploration abilities in reaching the perfect location and avoiding local optima generate considerable oscillations in the antenna positioning at a searching distance. The new positions of the antenna are ascertained through the utilization of Equation (10), which models the best location identification of antenna design.

$$\begin{aligned} C &= f_1 \cdot (G(e) + 2z) \\ G(e + 1) &= G(e) + C \cdot (2z + f_2) \end{aligned} \quad (10)$$

Here, f_1 and f_2 are denoted as the random variables with values between $[0, 2]$ and $[0, 1]$, respectively. Furthermore, C is a vector indicating the size of the elliptical area in which the antenna would search for possible location, and Z is an exponential variable with values between $[0, 1]$. If the response is unchanged after three repetitions, Equation (11) can modify the location of the antenna.

$$G(e + 1) = \text{Gaussian}(\mu p, \sigma) + r_1 \left(\frac{G(e) + 2z}{C} \right) \quad (11)$$

3.6.3. Exploitation: Best Solution of Antenna Design in the Suitable Parameter

Better solutions that are comparable to those previously found are identified because the antenna uses its local search capabilities. The behavior of natural waterwheels was replicated by the 8-port MIMO antenna designers through the stochastic assignment of favourable suitable parameters in locations to every MIMO antenna design in the population. According to the following formulas, the value of the objective function must be less than the value at the current position for the antenna design to be transferred. The BWPA's algorithmic architecture will also be an antenna design exhibited and explored, along with a schema explaining how it works. The sigmoid function below converts the continuous solution provided by the WPA algorithm into a binary solution of antenna design, where the most effective continuous solution is found using the continuous WPA method.

$$\begin{aligned} C &= f_3(ZG_{best}(e) + f_3G(e)) \\ G(e + 1) &= G(e) + ZC \end{aligned} \quad (12)$$

Here, $G(e)$ is denoted as the current solution at iteration e ; f_3 is denoted as the random variable with values between $[0, 2]$; e is the number of iterations; and G_{best} is the optimal answer. Similar to the investigation phase, the subsequent mutation is executed to prevent the solution from becoming mired in particular local minima if it fails to improve after three iterations. The next mutation, similar to the query phase, is intended to prevent the solution from becoming caught in a certain local minimum if it does not improve after three rounds.

$$G(e + 1) = (f_1 + z) \sin \left(\frac{X}{Y} \theta \right) \quad (13)$$

where $[-5, 5]$ is the range for the random variables X and Y .

3.6.4. Binarization of Antenna Design

A new version of the WPA was produced by adding more operators to the original WPA properties, which maximizes responses

in a discontinuous problem space. A transition from a continuous to a discrete form of solution representation and optimization is feasible via the initial phase, which involves the definition of transformation functions. This is crucial if the innovative method is to overcome obstacles in best antenna parameter selection. The new BWPA variation modifies the fitness function provided by the second model. To find the optimal option overall, the fitness of each alternative must be calculated, which offers a prerequisite for the fitness function to manage the particulars of the existing circumstance.

$$Binary = \left\{ \begin{array}{l} 1 \quad \text{if } sigmoid(G_{best}) \geq 0.5 \\ 0 \quad \text{otherwise} \end{array} \right\} \quad (14)$$

$$sigmoid(G_{Best}) = \frac{1}{1 + v^{-10(S_{Best}-0.5)}} \quad (15)$$

3.6.5. Fitness Function

The fitness function of the optimization algorithm is used to optimize the antenna parameters to enhance the gain and other performances of the antenna. A fitness function evaluation was required to discover the best answer to the best hyperparameter selection problem. As shown in the following equation,

$$Fitness(F) = \text{antenna design} \\ (\text{radiation pattern, gain, efficiency}) \quad (16)$$

It is concluded by suggesting that the antenna design parameters be optimised via a binary BWP optimization method. Table 6 depicts the step-by-step algorithm used to design the dual-band eight-port-MIMO antenna.

4. EXPERIMENTAL ANALYSIS

To validate the proposed geometry of the 8-port MIMO antenna with plus-shaped DGS and EBG metamaterials, the antenna model was simulated using HFSS simulation software. The simulation results were then compared to the desired antenna characteristics to ensure that the proposed geometry was able to achieve the desired isolation, mutual coupling, and reliability. The performance of the proposed antenna model was evaluated using several metrics such as diversity performances such as the TARC, MEG, and DG, as well as metrics such as gain, return loss, VSWR, radiation pattern, and AR. This evaluation shows the V2X communication capabilities of the recommended 8 port antenna in the following areas.

4.1. Performance Analysis

The proposed eight-port MIMO antenna with an EBG resonator is measured in terms of the performance criteria.

4.1.1. Return Loss

The return loss is defined by the following equation and is said to be a transmission line that indicates the power loss in the signal in decibels.

$$RL = 10 \log_{10} \left(\frac{K_a}{K_q} \right) \quad (17)$$

4.1.2. VSWR

The shading waves from the minimum to maximum voltage are called VSWR and can be calculated using the following equation.

$$V = \frac{M_{\max i}}{M_{\min i}} \quad (18)$$

4.1.3. Radiation Pattern

The relationship between the radiated power of the antenna and the radiation pattern is mathematically expressed as follows.

$$R_\theta = \frac{\sin \left(\frac{ZW \sin \theta \sin \phi}{2} \right)}{\frac{ZW \sin \theta \sin \phi}{2}} \cos \left(\frac{ZW}{2} \sin \theta \cos \phi \right) \cos \phi \quad (19)$$

4.1.4. DG

Calculating the DG parameter, a mathematical measure of the signal-to-noise ratio of the MIMO antennas, is possible via the subsequent equation:

$$D = 10 \sqrt{1 - |\rho_{eij}|^2} \quad (20)$$

4.1.5. TARC

The reflection coefficient of a MIMO antenna at various input phase angles is computed utilising TARC. The TARC is computed utilising the formula provided below.

$$T = \frac{\sqrt{\left(\left| (G_{xx} + G_{xy}^{jL\theta}) \right|^2 + \left| (G_{yx} + G_{yy}^{iL\theta}) \right|^2 \right)}}{\sqrt{2}} \quad (21)$$

Here, G_{yy}/G_{xx} is denoted as the reflection coefficient and G_{xy}/G_{yx} is denoted as the transition coefficient between ports.

4.1.6. MEG

In a multipath fading environment, MEG is defined as the ratio of average power received by the diversity antenna to average power received by the isotropic antenna. The next equation will provide a mathematical expression of (22).

$$M_A = 0.5 \mu_{prad} = 0.5 \left(1 - \sum_{y=1}^S |c_{Py}|^2 \right) \quad (22)$$

Here, S is denoted as the total counts of antennas; the y th radiation efficiency antenna is denoted by μ_{prad} ; and the active antenna is mentioned by c .

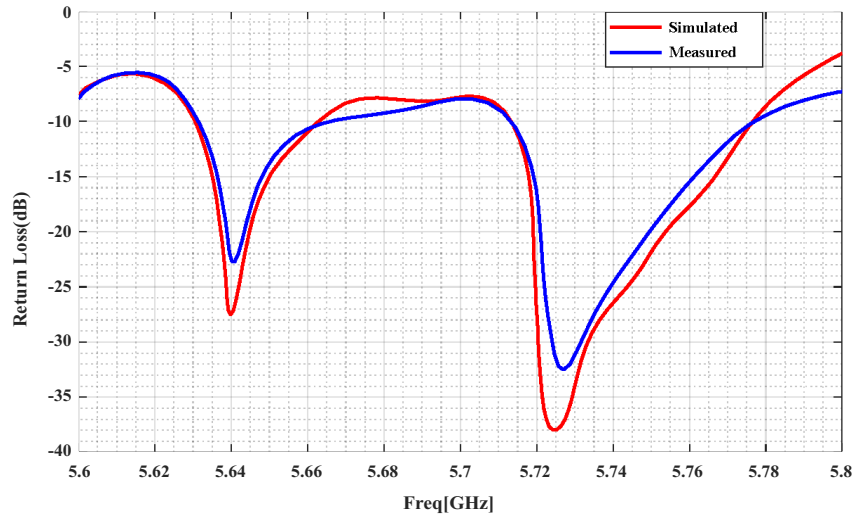


FIGURE 9. Analysis of return loss.

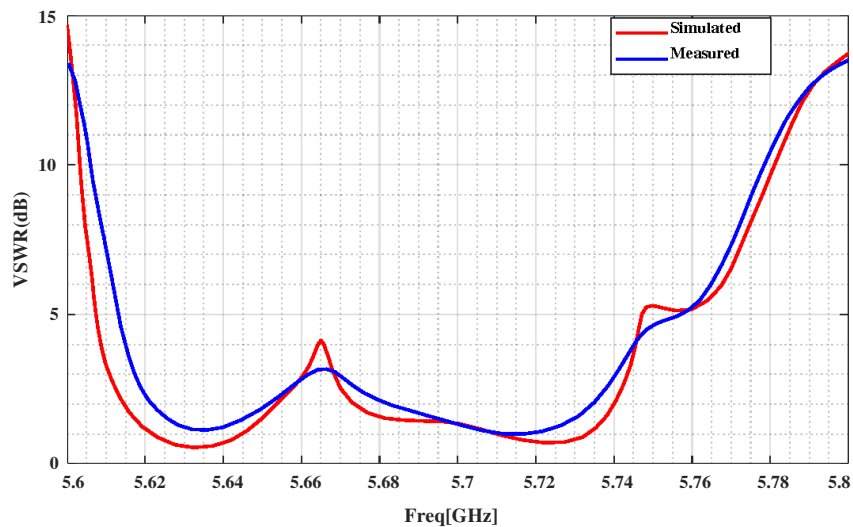


FIGURE 10. Analysis of VSWR.

4.1.7. ECC

The ECC is calculated taking into account the correlation between transmitting and receiving signals in antenna elements. In addition, the diversity of the antennas is measured using ECC.

$$E = \frac{|G_{xx}^* G_{xy} + G_{yx}^* G_{yy}|^2}{|1 - |G_{xx}|^2 - |G_{yx}|^2| |1 - |G_{yy}|^2 - |G_{xy}|^2|} \quad (23)$$

4.1.8. Axial Ratio

An axial ratio is the ratio of an electromagnetic wave’s minor to major axis or a circularly polarized antenna pattern. The following equation defines the axial ratio.

$$M = \left| \frac{Gk + 1}{Gk - 1} \right| \quad (24)$$

Here, linear polarization is denoted as the Gk , and M is denoted as the axial ratio.

4.2. Performance Evaluation of Suggested 8 port MIMO Antenna

The suggested 8 port MIMO antenna’s performance demonstrates that it can isolate a larger area than other commonly used antenna types. Figure 9 shows the evaluated return loss for the suggested antenna model.

In Figure 9, the return loss can be analyzed for the proposed model and can obtain values of -27.1064 dB at a resonating frequency of 5.63926 GHz and -37.9382 dB at a resonating frequency of 5.72526 GHz in the simulation results. The measured results can obtain values of -23.43 dB at 5.6413 GHz and -33.34 dB at 5.72945 GHz. In this analysis, the simulated results are matched with measured ones. The resonating frequencies and return loss values are close between the simulated and measured results, indicating a reasonable match between

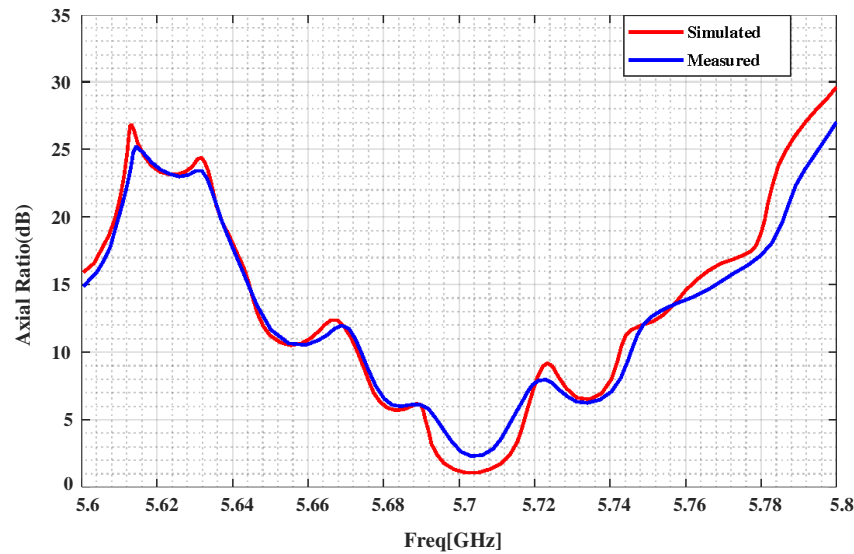


FIGURE 11. Axial ratio of the proposed model.

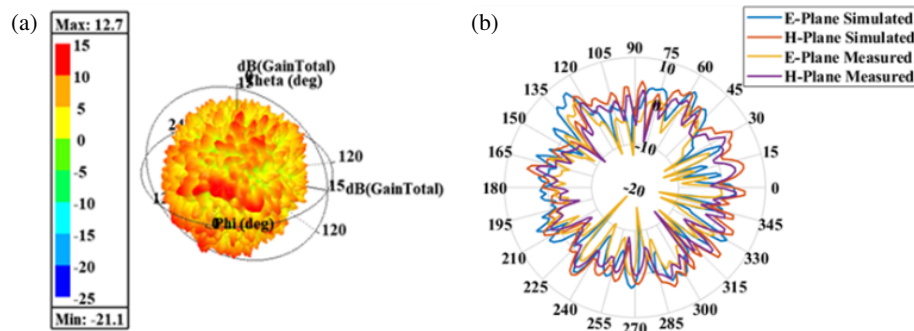


FIGURE 12. 3D Gain and 2D Gain for the first band of the eight-port MIMO antenna design.

them. This suggests that the proposed model is effective in predicting the behavior of the system. Figure 10 shows the evaluated VSWR for the proposed antenna model.

This figure shows the performance evaluation of VSWR for the proposed model with simulated and measured results at frequencies ranging from 5.6 GHz to 5.8 GHz. The proposed antenna model can obtain values between 1 and 2, which indicates good impedance matching and low signal reflection. This is desirable for antenna performance, as it means that more of the transmitted power is being received by the antenna.

Figure 11 shows the axial ratio of the antenna model, with a perfect value being 1 dB for an ideal antenna. The proposed antenna model has better performance in axial ratio analysis than a linearly polarized antenna with an axial ratio usually over 20 dB. However, the axial ratio of the proposed antenna model is between 5.6 dB and 5.8 dB, indicating linear polarization, with 1 dB indicating perfect polarization and an infinite axial ratio indicating a linearly polarized antenna. The 3D gain and 2D gain for the first band of the 8-port MIMO antenna design are shown in Figures 12(a) and 12(b).

Figure 12 shows the simulated and measured 3D and 2D gains for the first band of the proposed 8-port MIMO antenna design. The 3D gain curve has a maximum total gain

of 12.41 dB and a minimum gain of -24.63 dB, achieved in the metamaterial range of 5.6398 GHz. The 2D gain diagram for gain analysis is presented for the E and H planes, with the E plane given degree 0 and the H plane given degree 90. The 2D gain diagrams show the simulated and measured results for the E and H planes, with a maximum gain of 12.7 dB and a minimum gain of -21.1 dB. The simulated and measured results show a good agreement, indicating the reliability of the proposed antenna design. The 3D and 2D gain diagrams demonstrate excellent gain performance of the proposed MIMO antenna design. Figures 13(a) and 13(b) show the 2D and 3D gain plots for the second band of the eight-port MIMO antenna.

Figures 13(a) and 13(b) show the 3D and 2D gains for the second band of the proposed 8-port MIMO antenna design at 5.7242 GHz. The 3D gain curve has a maximum total gain of 10.7 dB and a minimum gain of -37.5 dB. The 2D gain diagrams for gain analysis are presented for the E and H planes, with the E plane given degree 0 and the H plane given degree 90. The 2D gain diagrams show the simulated and measured results for the E and H planes, with a maximum gain of 12.7 dB and a minimum gain of -21.1 dB. The simulated and measured results show a good agreement, indicating the reliability of the proposed antenna design. The 3D and 2D gain di-

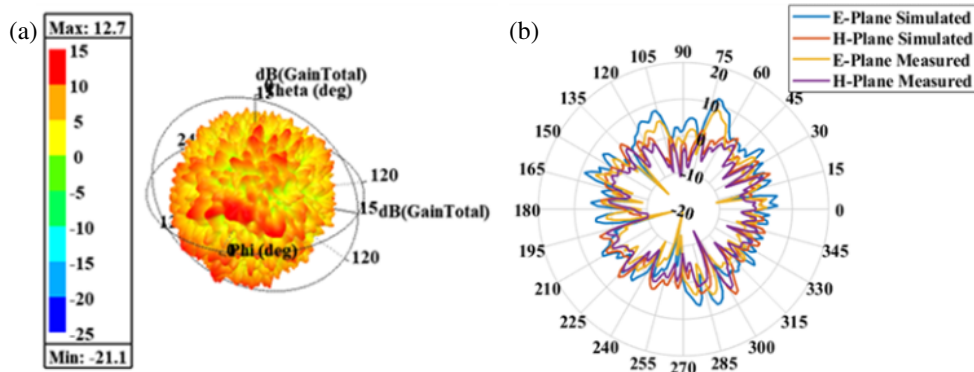


FIGURE 13. 3D Gain and 2D Gain for the second band of the eight-port MIMO antenna design.

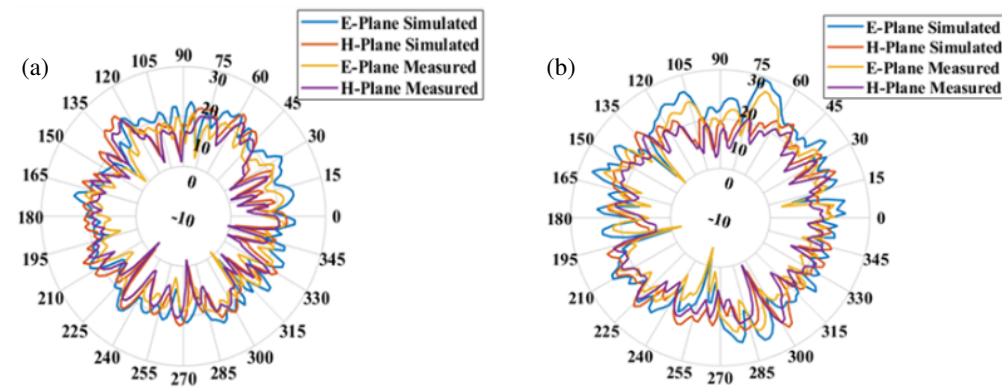


FIGURE 14. 2D Radiation pattern for the first band (a) and Second band (b) of the proposed model.

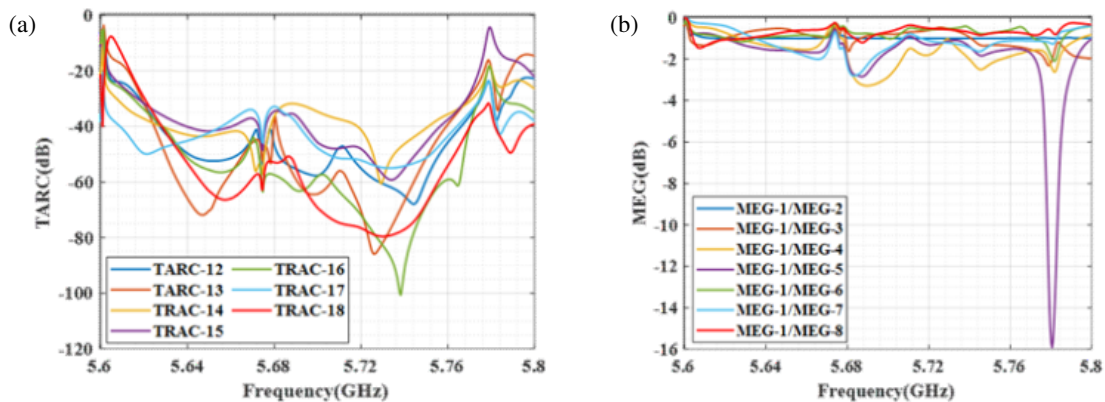


FIGURE 15. Examination of TARG and MEG of the proposed antenna.

agrams demonstrate the excellent gain performance of the proposed MIMO antenna design for the second band. Figure 14 shows the 2D radiation pattern for the first and second bands of the proposed MIMO antenna.

Figures 14(a) and 14(b) show the simulated and measured 2D radiation patterns for the first and second bands of the proposed MIMO antenna, respectively. The radiation patterns are presented for linearly polarized directivities in the H -plane (x - z) and E -plane (y - z) for the first band for a frequency range of 5.63926, and the second band for a frequency range of 5.72526 GHz. The figures demonstrate the excellent radiation properties of the proposed antenna, with high directivity and

low side lobes. Figure 15 shows an evaluation of TARG and MEG of the proposed antenna.

Figure 15(a) shows the evaluation of the eight-port MIMO antennas, TARC-12 to TARC-18. The TARC on port 18 reduces dual band frequencies by less than -60 dB or less than -65 dB. The effective reflection coefficient for the proposed 8-port MIMO antenna can be determined using the TARG measure. The MEG can be evaluated for the eight-port antenna model, as shown in Figure 15(b). Seven distinct port combinations of MEG-1/MEG-2, MEG-1/MEG-3, MEG-1/MEG-4, MEG-1/MEG-5, MEG-1/MEG-6, MEG-1/MEG-7, and MEG-1/MEG-8 can be evaluated. In MEG analysis, ports 1, 3, and

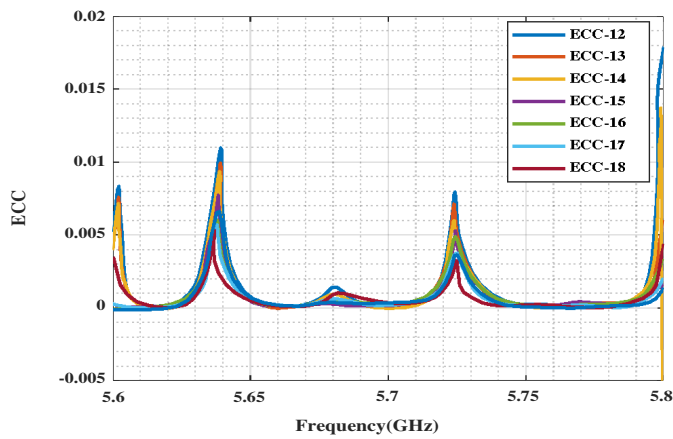


FIGURE 16. Analysis of the ECC proposed antenna.

7 can occur at less than -2 dB and -1 dB, respectively. ECC is examined in Figure 16 for the proposed eight-port antenna design.

Although the ECC started at 5.6 GHz, it can reach values above 5.8 GHz at its maximum frequency of 5.8 GHz. By measuring the ECC of an eight-port antenna in seven different configurations, namely ports 12, 13, 14, 15, 16, 17, and 18, an ECC < 0.25 dB can be determined. Figure 17 shows the diversity gain for the proposed 8-port antenna design.

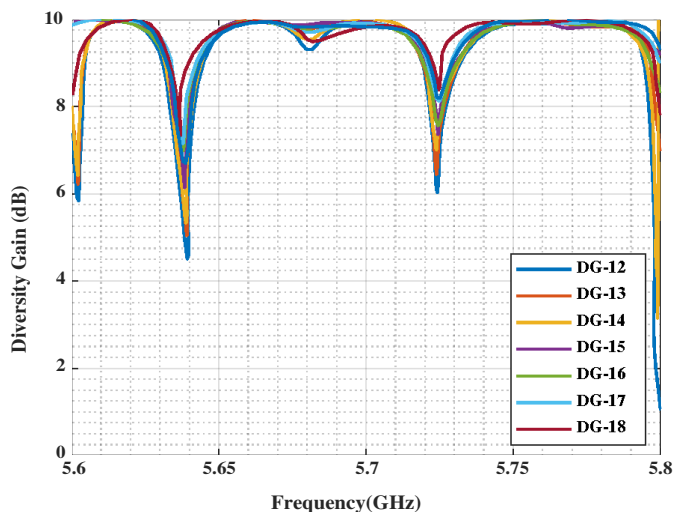


FIGURE 17. Analysis of diversity proposed antenna.

Figure 17 shows how the proposed antenna models DG, measured in decibels and applied to ports 12, 13, 14, 15, 16, 17, and 18, can improve the reliability and quality of wireless networks. In the frequency range of 5.75 GHz to 5.8 GHz, DG is less than 2.5 dB for the DG-12 port. DG can provide considerable gains of more than 10 dB within the recommended antenna bandwidth. Figure 18 shows the proposed CCL models.

An analysis of the CCL using seven ports, such as CCL 12 to CCL 18, is presented in Figure 18. Although the CCL was originally initiated at 5.6 GHz, it can reach values above 5.8 GHz at its maximum frequency of 5.8 GHz. The ECC of an eight-port antenna can be measured in seven different configurations to obtain a CCL > 0.25 dB. High values were thus achieved with

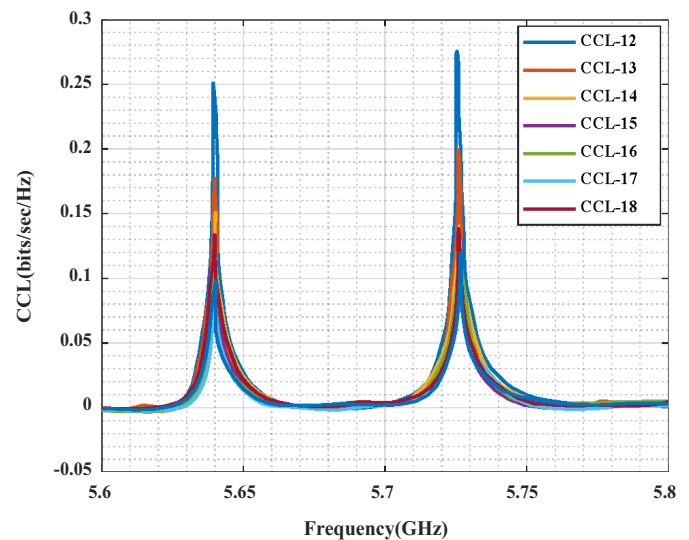


FIGURE 18. CCL of Proposed antenna model.

the proposed 8-port MIMO antenna. Figure 19 shows the proposed antenna isolation model.

The figure compares the simulated and measured isolations of an 8-port MIMO antenna for V2X applications. The antenna has high isolation, greater than -30 dB, which reduces interference. The proposed antenna design further enhances isolation to -60 dB in the 5.63–5.67 GHz range, improving V2X performance. The simulated and measured results are closely aligned, indicating the reliability of the proposed design.

Figure 20 displays the analysis of mutual coupling in an 8-port MIMO antenna for V2X applications. The graph shows the S -parameters, which represent the transmitted and received signal strengths by each antenna element. The proposed antenna design achieves a high isolation of -60 dB by minimizing the mutual coupling between the antenna elements, resulting in reduced interference and improved performance. The simulated and measured results show good agreement, indicating the reliability of the proposed antenna design. Figure 21 displays the surface current distribution in the proposed antenna design.

In Figure 21, the surface current distribution of the proposed antenna at a frequency of 5.6 GHz to 5.8 GHz is shown. The antenna consists of eight ports, and the decoupling structure ensures that the induced current is prevented from flowing to the surrounding patches. This is achieved by the proposed decoupling mechanism, which effectively isolates the MIMO antenna parts from each other. The current distribution in the antenna is predominantly located on the antenna patches, with a uniform distribution across the entire patch region. This uniform current distribution ensures efficient power transfer and minimizes the impact of mutual coupling on the overall performance of the MIMO antenna system. Finally, the decoupling structure in the proposed MIMO antenna plays a vital role in minimizing mutual coupling and improving the overall performance of the communication system. By analyzing the surface current distribution and optimizing the antenna design, it is possible to achieve high isolation and efficient power transfer between the antenna elements. The comparison table for different antenna models is analyzed under several performances such as

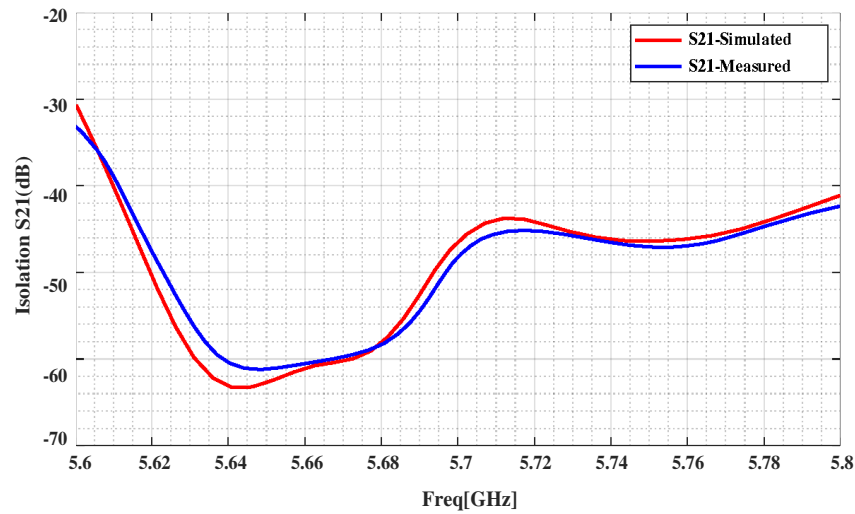


FIGURE 19. Analysis of isolation.

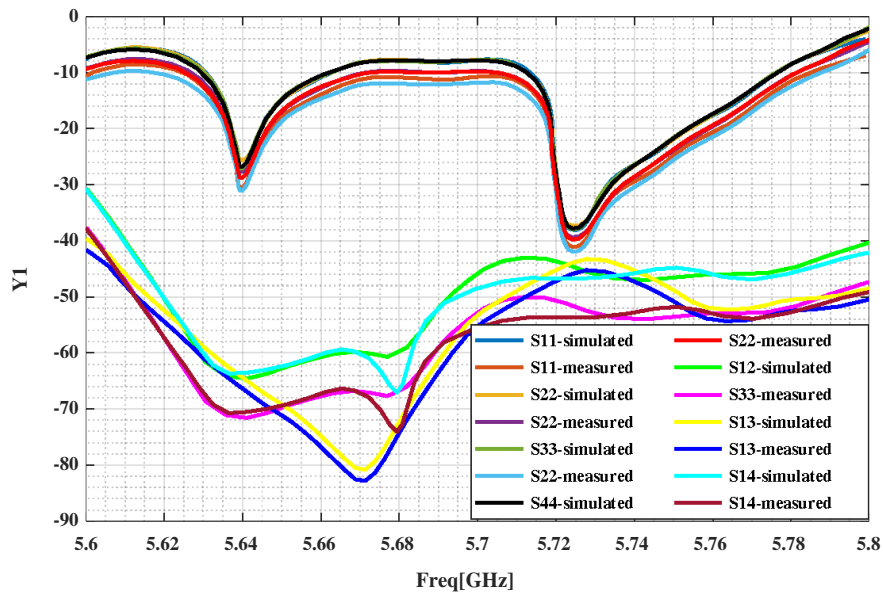


FIGURE 20. Analysis of mutual coupling.

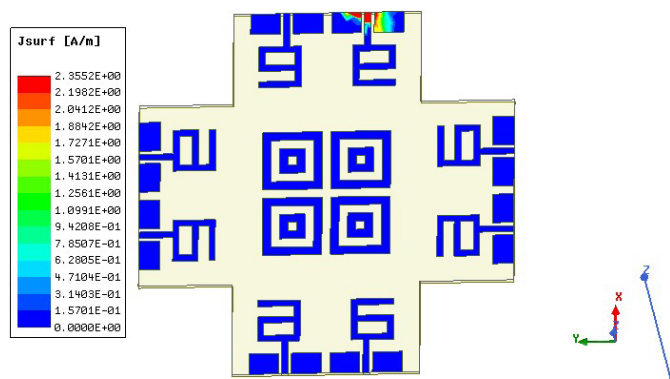


FIGURE 21. Analysis of surface current distribution.

frequency, substrate, band, return loss, ECC, and gain, which is represented in Table 7.

In this table, various existing models are analyzed to evaluate the performance of the proposed antenna design. Compared to existing designs, the proposed antenna has superior gain and overall performance. This comparison analysis shows that the proposed MIMO antenna outperforms other existing models, with lower return loss and higher ECC. The proposed antenna can produce superior outcomes in this work.

4.3. Discussion

In recent years, V2X communication technologies have advanced with the integration of MIMO systems. MIMO allows for electronic control of signal propagation, enhancing data transmission and reception efficiency without additional capacity. However, close proximity of antennas can lead to interference issues, prompting researchers to develop MIMO antennas with minimal interference. Various techniques have been ex-

TABLE 7. Comparison analysis of existing design and proposed design.

Refer	Antenna design	Dimension λ_0	Frequency (GHz)	Band	Substrate	Gain (dB)	Return loss (dB)	ECC
[48]	Four ports	$1.1 \lambda_0 \times 1.2 \lambda_0$	4.8	Single	FR-4	2.8	-30	<0.01
[49]	Four ports	$0.10 \lambda_0 \times 12 \lambda_0$	5	Single	FR-4	5.9	-30.1	<0.0002
[50]	Four ports	$95 \lambda_0 \times 27 \lambda_0$	4.5 5	Dual	FR-4	7.6 8.32	-19 -20.4	<0.4
[35]	Two port	$60 \lambda_0 \times 86 \lambda_0$	4.7	Single	Ro4003, FR-4	7.8	-20	<0.005
[40]	Eight port	$0.16 \lambda_0 \times 0.16 \lambda_0$	24.25 29.5	Dual	FR-4	9.5	-28 -30.4	<0.06
[41]	Eight port	$0.1 \lambda_0 \times 0.1 \lambda_0$	3.3 3.8	Dual	FR4	8.44	-31.8 -34.89	<0.09
[42]	Eight port	$0.2 \lambda_0 \times 0.2 \lambda_0$	3.3 4.2	Dual	FR-4	8.934	-28.27 -30.83	<0.05
[43]	Eight port	$0.05 \lambda \times 0.16 \lambda$	3.5 5.5	Dual	FR-4	9.8	-30.4 -34.5	<0.001
Proposed	Eight port	$80 \lambda_0 \times 80 \lambda_0$	5.64 5.73	Dual	polyimide	12.41 10.7	-36.01, -39	<0.025

plored to reduce interference. To mitigate interference and improve performance, a novel dual-band 8-port MIMO antenna based on metamaterial is under development for V2X applications. This design utilizes advanced metamaterial structures and algorithms to achieve very low interference. The antenna array facilitates seamless communication in both licensed and unlicensed frequency bands, enabling efficient communication within the V2X network.

To validate the proposed geometry of the 8-port MIMO antenna with a plus-shaped DGS and EBG metamaterials, the antenna model was simulated using HFFS simulation software. The simulation results were then compared to the desired antenna characteristics to ensure that the proposed geometry was able to achieve the desired isolation, mutual coupling, and reliability. The proposed 8-port MIMO antenna achieved a TARC of less than -10 dB, indicating good matching between the antenna and the transmission line. The MEG of the proposed antenna was greater than 8 dBi, indicating high gain and directivity. The DG of the proposed antenna was greater than 10 dB, indicating excellent diversity performance. The proposed antenna also achieved a gain of 5.5 dBi, a return loss of less than -10 dB, a VSWR of less than 1.5, and an AR (Axial Ratio) of less than 3 dB. The radiation pattern of the proposed antenna was evaluated and showed good directivity and coverage.

Overall, the proposed 8-port MIMO antenna with a plus-shaped DGS and EBG metamaterials was able to achieve the desired isolation, mutual coupling, and reliability, as demonstrated by the simulation results. The proposed antenna is well suited for V2X applications in the 5.6 GHz–5.8 GHz frequency range, and further optimization and fine-tuning of the antenna design can be performed to potentially reduce its size and weight while maintaining its performance characteristics.

5. CONCLUSION

In conclusion, this paper presents a novel dual-band, linearly polarized, eight-port MIMO antenna design for V2X communications, operating in the 5.6 GHz–5.8 GHz frequency range. The antenna design incorporates the use of a polyimide substrate, CPW, plus-shaped DGS, and EBG metamaterial to

achieve high isolation, low mutual coupling, and improved transmission rates. The proposed design is optimized using the BWP optimization method, which is a binary-based optimization algorithm inspired by the waterwheel plant's water distribution mechanism. The BWP algorithm is used to optimize the design parameters of the 8-port MIMO antenna, leading to improved isolation, mutual coupling, and reliability compared to existing models. The antenna achieves an ECC of less than 0.25 dB, demonstrating its potential for V2X applications. The proposed antenna design has the potential to significantly improve the communication rate between vehicles, which is essential for the success of V2X applications. The design also offers the potential for miniaturization, which could lead to reduced size and weight of the device.

Future work should focus on optimizing and fine-tuning the design of the antenna to potentially reduce its size further. This could involve exploring different design possibilities and strategies, conducting more detailed simulations and experiments to evaluate the performance of various antenna designs and configurations, and exploring new materials and manufacturing techniques that can help to optimize the overall performance and efficiency of the antenna. Additionally, alternative metamaterials for the antenna could lead to improvements in performance metrics such as gain, radiation efficiency, bandwidth, and isolation between antenna elements. Overall, this paper presents a promising antenna design for V2X communications that has the potential to significantly improve communication rates and reliability.

REFERENCES

- [1] Vasu Babu, K., S. Kokkirigadda, and S. Das, "Design and simulation of dual-band MIMO antenna for radar and Sub-6-GHz 5G applications," in *Futuristic Communication and Network Technologies: Select Proceedings of VICFCNT 2020*, 289–295, Springer Singapore, 2022.
- [2] Wu, Y., D. Xu, D. W. K. Ng, W. Gerstacker, and R. Schober, "Movable antenna-enhanced multiuser communication: Optimal discrete antenna positioning and beamforming," *ArXiv Preprint ArXiv:2308.02304*, 2023.

- [3] Björnson, E., J. G. Andrews, and M. Debbah, “Massive MIMO for 6G: Where do we stand?” *IEEE Journal on Selected Areas in Communications*, Vol. 36, No. 2, 223–238, Feb. 2023.
- [4] Kim, S. J., J. H. Cho, and Y. Choi, “OFDM for 6G wireless communication systems: Recent advances and challenges,” *IEEE Communications Magazine*, Vol. 61, No. 2, 66–73, Feb. 2023.
- [5] Andrews, J. G., S. Buzzi, W. Choi, S. V. Scheluter, A. Lozano, A. L. Swindlehurst, and S. Madden, “What will 6G be?” *IEEE Journal on Selected Areas in Communications*, Vol. 36, No. 2, 120–136, Feb. 2023.
- [6] Debbah, M., A. Lozano, and R. W. H. Jr., “Dynamic spectrum access for 6G and beyond,” *IEEE Wireless Communications*, Vol. 28, No. 6, 20–27, Dec. 2023.
- [7] Watanabe, T., T. Ohta, and M. Nakagawa, “Spectrum sharing technologies for 6G and beyond,” *IEEE Wireless Communications*, Vol. 28, No. 6, 40–47, Dec. 2023.
- [8] Debbah, M., A. Lozano, and R. W. H. Jr., “Dynamic spectrum access for 6G and beyond,” *IEEE Wireless Communications*, Vol. 28, No. 6, 20–27, Dec. 2023.
- [9] Andrews, J. G., S. Buzzi, W. Choi, S. V. Scheluter, A. Lozano, A. L. Swindlehurst, and S. Madden, “What will 6G be?” *IEEE Journal on Selected Areas in Communications*, Vol. 36, No. 2, 120–136, Feb. 2023.
- [10] Islam, S. M. H., M. A. Islam, and M. R. Islam, “MIMO antenna systems: Analysis, design and applications,” *Springer Science & Business Media*, 1–20, 2020.
- [11] Zhang, J., Y. Zhang, and Y. Zhang, “Frequency reconfigurable antenna for wireless communication systems,” *IEEE Transactions on Antennas and Propagation*, Vol. 68, No. 6, 3757–3766, Jun. 2020.
- [12] Islam, S. M. H., M. A. Islam, and M. R. Islam, “MIMO antenna systems: Analysis, design and applications,” *Springer Science & Business Media*, 21–40, 2020.
- [13] Liu, Y., X. Yang, Y. Jia, and Y. J. Guo, “A low correlation and mutual coupling MIMO antenna,” *IEEE Access*, Vol. 7, 127 384–127 392, 2019.
- [14] Khabba, A., J. Amadid, S. Ibnyaich, and A. Zeroual, “Pretty-small four-port dual-wideband 28/38 GHz MIMO antenna with robust isolation and high diversity performance for millimeter-wave 5G wireless systems,” *Analog Integrated Circuits and Signal Processing*, Vol. 112, No. 1, 83–102, 2022.
- [15] Raj, T., R. Mishra, P. Kumar, and A. Kapoor, “Advances in MIMO antenna design for 5G: A comprehensive review,” *Sensors*, Vol. 23, No. 14, 6329, 2023.
- [16] Ahmad, I., W. Tan, Q. Ali, and H. Sun, “Latest performance improvement strategies and techniques used in 5G antenna designing technology, a comprehensive study,” *Micromachines*, Vol. 13, No. 5, 717, 2022.
- [17] Ali, A., M. E. Munir, M. M. Nasralla, M. A. Esmail, A. J. A. Al-Gburi, and F. A. Bhatti, “Design process of a compact Tri-Band MIMO antenna with wideband characteristics for sub-6 GHz, Ku-band, and Millimeter-Wave applications,” *Ain Shams Engineering Journal*, Vol. 15, No. 3, 102579, 2024.
- [18] Vaigandla, K. K. and D. N. Venu, “Survey on massive MIMO: Technology, challenges, opportunities and benefits,” *YMER*, Vol. 20, No. 11, 271–282, 2021.
- [19] Huang, C., S. Hu, G. C. Alexandropoulos, A. Zappone, C. Yuen, R. Zhang, M. D. Renzo, and M. Debbah, “Holographic MIMO surfaces for 6G wireless networks: Opportunities, challenges, and trends,” *IEEE Wireless Communications*, Vol. 27, No. 5, 118–125, 2020.
- [20] Hussain, N., K. Aljaloud, R. Hussain, A. H. Alqahtani, Z. U. Khan, F. A. Tahir, and Q. H. Abbasi, “Dual-sense slot-based CP MIMO antenna with polarization bandwidth reconfigurability,” *Scientific Reports*, Vol. 13, No. 1, 16132, 2023.
- [21] Chowdhury, A. and P. Ranjan, “A novel PIN diode-based frequency reconfigurable patch antenna with switching between the mid-5G and high-5G frequency band,” *International Journal of Microwave and Wireless Technologies*, 1–10, 2023.
- [22] Kumari, P. and S. Dwari, “Reconfigurable MIMO antenna: Previous advancements and the potential for future wireless communication,” *International Journal of Microwave and Wireless Technologies*, 1–11, 2023.
- [23] Kumari, R. and M. Angira, “RF-MEMS capacitive switches: enabling transition towards 5G/B5G applications,” *International Journal of Information Technology*, Vol. 15, No. 7, 3889–3897, 2023.
- [24] Kareem, Q. H., R. A. Shihab, and H. H. Kareem, “Compact dual-polarized reconfigurable MIMO antenna based on a varactor diode for 5G mobile terminal applications,” *Progress In Electromagnetics Research C*, Vol. 137, 185–198, 2023.
- [25] Barik, R. K. and S. Koziel, “Microfluidically frequency-reconfigurable compact self-quadruplexing tunable antenna with high isolation based on substrate integrated waveguide,” *Scientific Reports*, Vol. 14, No. 1, 920, 2024.
- [26] Durukan, T. and Y. Altuncu, “A compact 4×4 reconfigurable MIMO antenna design with adjustable suppression of certain frequency bands within the UWB frequency range,” *AEU — International Journal of Electronics and Communications*, Vol. 170, 154848, 2023.
- [27] Mudda, S. and K. M. Gayathri, “Frequency reconfigurable ultra-wide band MIMO antenna for 4G/5G portable devices applications,” *International Journal on Emerging Technologies*, Vol. 11, No. 3, 486–490, 2020.
- [28] Sabek, A. R., W. A. E. Ali, and A. A. Ibrahim, “Minimally coupled two-element MIMO antenna with dual band (28/38 GHz) for 5G wireless communications,” *Journal of Infrared, Millimeter, and Terahertz Waves*, Vol. 43, No. 3, 335–348, 2022.
- [29] Liu, X., Q. Chen, and J. J. He, “Design and analysis of a compact MIMO antenna for 5G smartphones,” *IEEE Antennas and Wireless Propagation Letters*, Vol. 19, 1564–1567, 2020.
- [30] Mohammed, D. J. A., “Designing an effective MIMO antenna for 5G,” 2023.
- [31] Virothu, S. and M. S. Anuradha, “Flexible CP diversity antenna for 5G cellular Vehicle-to-Everything applications,” *AEU — International Journal of Electronics and Communications*, Vol. 152, 154248, 2022.
- [32] Yang, S., L. Liang, Z. Li, and W. Wang, “Ultra-wideband MIMO circularly-polarized cube antenna with characteristic mode analysis for wireless communication and sensing,” *IEEE Internet of Things Journal*, Vol. 11, No. 7, 12 192–12 202, 2023.
- [33] Sial, M. N., Y. Deng, J. Ahmed, A. Nallanathan, and M. Dohler, “Stochastic geometry modeling of cellular V2X communication over shared channels,” *IEEE Transactions on Vehicular Technology*, Vol. 68, No. 12, 11 873–11 887, 2019.
- [34] Rasheed, I., “An effective approach for initial access in 5G-millimeter wave-based Vehicle to Everything (V2X) communication using improved genetic algorithm,” *Physical Communication*, Vol. 52, 101619, 2022.
- [35] Fu, Y., T. Shen, and J. Dou, “Mutual coupling reduction of a multiple-input multiple-output antenna using an absorber wall and a combline filter for V2X communication,” *Sensors*, Vol. 23, No. 14, 6355, 2023.
- [36] Ez-Zaki, F., H. Belahrach, G. Abdelilah, S. Ahmad, A. Khabba, K. Aitbelaid, A. Ghaffar, and M. I. Hussein, “Double Negative (DNG) Metamaterial based Koch fractal MIMO antenna de-

- sign for sub-6 GHz V2X communication,” *IEEE Access*, Vol. 11, 77 620–77 635, 2023.
- [37] Chung, K. L., L. Chen, G. Lai, K. Zheng, Z. Wang, H. Cui, and B. Feng, “Three-element circularly polarized MIMO antenna with self-decoupled probing method for B5G-V2X communications,” *Alexandria Engineering Journal*, Vol. 70, 553–567, 2023.
- [38] Aliqab, K., A. Armghan, M. Alsharari, and M. H. Aly, “Highly decoupled and high gain conformal two-port MIMO antenna for V2X communications,” *Alexandria Engineering Journal*, Vol. 74, 599–610, 2023.
- [39] Rakluea, P., N. Wongsin, C. Mahatthanajatuphat, P. Aroonmitr, T. Jangjing, C. Rakluea, W. Chanwattanapong, and N. Chudpooti, “Flexible thin film-based triple port UWB MIMO antenna with modified ground plane for UWB, WLAN, WiMAX, WPAN and 5G applications,” *IEEE Access*, Vol. 11, 107 031–107 048, 2023.
- [40] Wong, K.-L., S.-E. Hong, Y.-S. Tseng, and W.-Y. Li, “Low-profile compact 8-port MIMO antenna module and its 1×2 array for 6G 16×8 device MIMO application,” *IEEE Access*, Vol. 11, 137 011–137 024, 2023.
- [41] Sufyan, A., K. B. Khan, X. Zhang, T. A. Siddiqui, and A. Aziz, “Dual-band independently tunable 8-element MIMO antenna for 5G smartphones,” *Heliyon*, Vol. 10, No. 4, E25712, 2024.
- [42] Guo, J., S. Zhang, C.-Z. Han, and L. Zhang, “Combined open-slot and monopole 8×8 high-isolation broadband MIMO antenna system for sub-6 GHz terminals,” *International Journal of Antennas and Propagation*, Vol. 2023, 2023.
- [43] Khan, A., A. Wakeel, L. Qu, and Z. Zahid, “Dual-band 8×8 MIMO antenna with enhanced isolation and efficiency for 5G smartphone applications,” *AEU — International Journal of Electronics and Communications*, Vol. 163, 154600, 2023.
- [44] Sujanth Narayan, K. G., J. A. Baskaradas, and D. R. Kumar, “Design of a CPW-fed compact MIMO antenna for next generation vehicle to everything (V2X) communication,” *Wireless Personal Communications*, Vol. 120, No. 3, 2179–2200, 2021.
- [45] Aliqab, K., A. Armghan, M. Alsharari, and M. H. Aly, “Highly decoupled and high gain conformal two-port MIMO antenna for V2X communications,” *Alexandria Engineering Journal*, Vol. 74, 599–610, 2023.
- [46] Ko, M., H. Lee, and J. Choi, “Planar LTE/sub-6 GHz 5G MIMO antenna integrated with mmWave 5G beamforming phased array antennas for V2X applications,” *IET Microwaves, Antennas & Propagation*, Vol. 14, No. 11, 1283–1295, 2020.
- [47] Abdelhamid, A. A., S. K. Towfek, N. Khodadadi, A. A. Alhus-san, D. S. Khafaga, M. M. Eid, and A. Ibrahim, “Waterwheel plant algorithm: A novel metaheuristic optimization method,” *Processes*, Vol. 11, No. 5, 1502, 2023.
- [48] Ali, H., X.-C. Ren, I. Bari, M. A. Bashir, A. M. Hashmi, M. A. Khan, S. I. Majid, N. Jan, W. U. K. Tareen, and M. R. Anjum, “Four-port MIMO antenna system for 5G n79 band RF devices,” *Electronics*, Vol. 11, No. 1, 35, 2021.
- [49] Saadh, A. W. M., K. Ashwath, P. Ramaswamy, T. Ali, and J. Anguera, “A uniquely shaped MIMO antenna on FR4 material to enhance isolation and bandwidth for wireless applications,” *AEU — International Journal of Electronics and Communications*, Vol. 123, 153316, 2020.
- [50] Upadhyaya, T., I. Park, R. Pandey, U. Patel, K. Pandya, A. De-sai, J. Pabari, G. Byun, and Y. Kosta, “Aperture-fed quad-port dual-band dielectric resonator-MIMO antenna for Sub-6 GHz 5G and WLAN application,” *International Journal of Antennas and Propagation*, Vol. 2022, 1–13, 2022.